Journal of Ceramic Processing Research. Vol. 25, No. 4, pp. 490~498 (2024)
(Received 8 October 2023, Received in revised form 14 December 2023, Accepted 3 January 2024)
https://doi.org/10.36410/jcpr.2024.25.4.490

J O U R N A L O F
Ceramic Processing Research

Quasi-nanocrystalline ZrB_2 powder synthesized by salt-assisted combustion and its formation mechanism

Faqi Zhan[a,*], Ru Bai[a], Xiao Liu[a], Ke Xu[a], Hua Zhang[a], Min Zhu[a], Yuehong Zheng[a], Shipeng Xu[b], Jie Sheng[a] and Peiqing La[a,*]

[a]*State Key Laboratory of Advanced Processing and Recycling of Nonferrous Metals, Lanzhou University of Technology, Lanzhou 730050, China*

[b]*Gansu Key Laboratory of Solar Power System Engineering, Jiuquan Vocational and Technical College, Jiuquan 735000, China*

Nanoscale ceramic powders are very important for sintering densification and deviceization. A new salt-assisted combustion synthesis process was used to prepare pure quasi-nanocrystalline zirconium diboride (ZrB_2) powder on a large scale. The ZrO_2-B_2O_3-Mg system with single NaCl salt and NaCl-KCl mixed salts as diluents was adopted to prepare ZrB_2 powders. The results show that high-purity ZrB_2 quasi-nanocrystalline powder with average size of ~105 nm and purity of 99.24% was obtained by adding molten salts diluent. The impurity mainly existed in the form of $Mg_{0.2}Zr_{0.8}O_{1.8}$ phase and $Mg_3B_2O_6$ phase. The effects of diluent content and type on the adiabatic temperature, powder purity, particle size and microstructure of the system were studied. This work will provide theoretical basis and technical support for large-scale preparation of boride nano-ceramic powders.

Keywords: Salt-assisted combustion, ZrB_2 nanopowders, Molten salt diluent, Formation mechanism.

Introduction

The boride ceramic materials, known as ultra-high temperature ceramics, exhibit exceptional physical and mechanical properties characterized by high melting points and hardness. They also demonstrate remarkable impact and wear resistance, excellent resistance to chemical agents, as well as a high capacity for neutron absorption [1-3]. Zirconium diboride (ZrB_2) is an ultra-high temperature ceramic material with great development prospect. It has high melting point, high hardness and strength, high thermal conductivity and electric conductivity [4-6], good oxidation resistance, wear resistance and corrosion resistance [7, 8]. Owing to these excellent properties, ZrB_2 is widely used in propulsion materials, electrodes, thermocouples, high temperature structural ceramic materials, anti-corrosion and wear-resistant coating materials and cutting tools in aerospace [9-13]. However, the development and application of most high melting point compounds such as ZrB_2 are limited by the poor sintering performance [14]. The main reason is that the strong covalent bond, low self-diffusion coefficient and large particle size in the material jointly inhibit the diffusion and degradation of grains [15]. However, the preparation of ZrB_2 powder with smaller particle size and higher surface energy can well solve this problem [16, 17].

At present, the commonly used preparation methods of ZrB_2 are carbothermal reduction method [18, 19], sol-gel method (Sol-Gel) [20, 21], self-propagating high temperature synthesis method (SHS) [22, 23], salt-assissed combustion synthesis [24, 25], mechanical alloying (MA) [26, 27], etc. In recent years, Gye et al. [28] used ZrO_2 and B_4C as raw materials to synthesize submicron ZrB_2 powder with minimum particle size of 245 nm by carbothermal reduction method. Hossein et al. [29] prepared ZrB_2 powders with average particle size less than 250 nm by sol-gel method using $ZrCl_4$ and H_3BO_3 as raw materials. Mustafa et al. [30] used ZrO_2, B_2O_3 and C as raw materials to prepare ZrB_2 powder by mechanical alloying. The crystallite size was 0.5~1.0 μm. Wang et al. [31] added a diluent NaCl into the raw materials of ZrO_2 and amorphous B, and synthesized ZrB_2 powder with an average particle size of 500 nm by salt-assisted combustion. According to recent study, most of the reported ZrB_2 powder particle size is above 250 nm, which does not really reach the nanometer level. Therefore, large-scale preparation of ZrB_2 nanopowder (~100 nm) is technical bottleneck.

In this paper, ZrO_2-B_2O_3-Mg system was adopted by salt-assisted combustion synthesis. By regulating thermodynamic [32, 33] and kinetic conditions [34, 35] via adding single NaCl and mixed NaCl-KCl salt as diluents, high purity quasi-nanocrystalline ZrB_2 powder with the average particle size of ~100 nm was obtained.

*Corresponding author:
Tel : +86 15209310025
Fax: +86 15209310025
E-mail: zhanfaqi@lut.edu.cn (Faqi Zhan);
pqla@lut.edu.cn (Peiqing La)

The effect of the inert diluent on the purity and particle size of ZrB_2 and its mechanism were investigated.

Material and Methods

Material

The experimental materials were shown in Table 1. The total chemical reaction equation is as follows:

$$ZrO_2 + B_2O_3 + 5Mg + w\text{NaCl/NaCl-KCl} = 5MgO + ZrB_2 + w\text{NaCl/NaCl-KCl} \quad (1)$$

ZrO_2, B_2O_3 and Mg powders were mixed at the molar ratio of 1:1:6.25 (with 25% excess of Mg). The mass percent w of the diluent was 0 wt.%, 50 wt.%, 60 wt.%, 70 wt.% of the total mass of the material (excluding excess Mg). The mixed powder was ball milled for 8 h. ZrB_2 powder was synthesized by self-propagating reaction in a self-designed combustion synthesis furnace under the protection of 2.0 MPa argon [36, 37]. After natural cooling of sample in the reactor, the black sample was taken out and crushed. The reaction products need to be purified to completely remove MgO and residual salts by washing with 3.0 mol/L hydrochloric acid and distilled water. Finally, the product was dried in a vacuum oven at 70 °C for 12 h.

Characterization methods

The products before and after leaching were identified by D/MAX-2400 X-ray Diffractometer (XRD) with copper target K_α as radiation source. The particle size and microstructure of ZrB_2 powder were analyzed by JSM-6700 Scanning Electron Microscope (SEM) and JEM-2010 Transmission Electron Microscope (TEM). The particle size distribution of the samples was analyzed by Image-Pro Plus 6.0 image statistical software. The specific surface area of sample was measured by JW-BK200C specific surface and pore size analyzer (BET). The surface element content and chemical valence of the samples were determined by Shimadzu AXIS SUPRA X-ray Photoelectron Spectrometer (XPS).

Table 1. The experimental materials.

Materials	Purity (wt.%)	Impurity	Specifications
ZrO_2	>99.5	O, S, Al etc.	1 μm
B_2O_3	>98.0	-	1 μm
Mg	>99.5	Cl, S, O etc.	<200 mesh
KCl	>99.5	Na, SO_4^{2-}, Fe	<200 mesh
NaCl	>99.5	Mg, K, Fe, SO_4^{2-}	<200 mesh

Results and Discussion

Thermodynamic calculation of system

The Gibbs energy ΔG of the possible reactions (Table 2) in ZrO_2-B_2O_3-Mg system was calculated, and the relationship curve of ΔG-T of each reaction was presented in Fig. 1. The relevant data were referred to the Handbook of thermodynamics [38].

Fig. 1 showed the change trend of ΔG in each reaction with temperature. It could be seen that the ΔG was less than zero in the temperature range of 298 K to 1800 K,

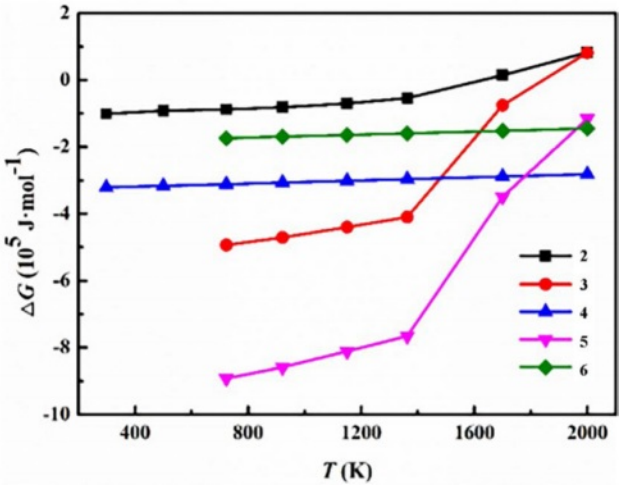

Fig. 1. Relationship of ΔG-T in the ZrO_2-B_2O_3-Mg system.

Table 2. Standard Gibbs energy change of reaction in ZrO_2-B_2O_3-Mg system.

No.	Reaction	A+BT / (J·mol^{-1})	Temperature region / K
(2)	$2Mg + ZrO_2(s) = Zr(s) + 2MgO(s)$	-110460+31.48T	298~922
		-127140+49.34T	922~1363
		-373400+228.28T	1363~2000
(3)	$3Mg + B_2O_3(l) = 2B(s) + 3MgO(s)$	-574890+112.74T	723~922
		-599910+139.50T	922~1363
		-969300+525.66T	1363~2000
(4)	$Zr(s) + 2B(s) = ZrB_2(s)$	-328000+23.4T	298~2125
(5)	$ZrO_2 + B_2O_3(l) + 5Mg = ZrB_2 + 5MgO$	-1013350+167.62T	723~922
		-1055050+212.24T	922~1363
		-1670700+777.34T	1363~2000
(6)	$3MgO + B_2O_3(l) = Mg_3B_2O_6$	-190023.62+22.74T	723~2316

which indicated that the reaction could be spontaneous. In these reactions, ΔG of reaction (5) was the most negative. This indicated that the positive trend of reaction (5) was the largest, and ZrB_2 and MgO formed by the reaction were the most stable phases. In addition, the three stages of reaction (2), (3) and (4) which constitute reaction (5) were spontaneous.

In addition, the ΔG of reaction (2) and (3) was greater than zero as the temperature exceeded 1800 K, and it was likely that the inverse reaction would occur. Inadequate magnesium thermal reduction resulted in residual ZrO_2 or the formation of intermediate product $Zr_xMg_yO_z$ [39, 40]. Further, impurity phases were generated in reactions (6), and ΔG was slightly higher than that of reaction (3). So the $Mg_3B_2O_6$ was inevitably generated in the reaction [41]. In conclusion, it was necessary to consider that the reaction temperature was too high, which leaded to reverse magnesium thermal reduction and even the formation of impurities in the early stage of experimental design.

The adiabatic temperature T_{ad} refers to the maximum temperature that the system can reach under ideal adiabatic conditions. There is no heat exchange between the system and the outside world, the reaction is strictly in accordance with the reaction equation and there is no leftover of the reactants at standard atmospheric pressure, which is the ideal adiabatic conditions [42]. According to experience, spontaneous reactions can be maintained at $T_{ad} \geq 1800$ K. If $T_{ad} < 1800$ K, preheating, chemical furnace and thermal explosion can be used for heating system.

The adiabatic temperature calculation formula of the system [43]:

$$-\Delta H^{\theta}_{298} = \int_{298}^{T_{tr}} nC_p(products)\,dT + n\Delta H_{tr} + \int_{T_{tr}}^{T_{ad}} nC_p(products)dT \quad (2)$$

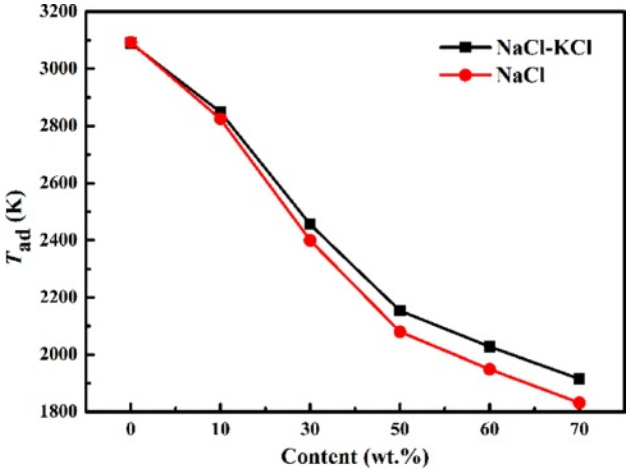

Fig. 2. Effect of different diluent additions on adiabatic temperature.

Where ΔH^{θ}_{298} is the standard molar enthalpy of formation of the product at 298 K; C_p is the molar constant pressure heat capacity of the product; T_{tr} is the melting point of the product, and ΔH_t is the melting heat of the product. C_p can be calculated as:

$$C_p = A_1 + A_2 \times 10^{-3}\,T + A_3 \times 10^{5} T^{2} + A_4 \times 10^{-6} T^{2} \quad (3)$$

Where A_1, A_2, A_3 and A_4 are the coefficients of each temperature term in the constant pressure molar heat capacity calculation formula of matter, which are obtained by querying the thermodynamic manual [38]. Thus, the adiabatic temperature of the system with different diluent additions was calculated by Formula (4):

$$-\Delta H^{\theta}_{298} = \int_{298}^{T_{ad}} nC_p(MgO + ZrB_2)dT + \int_{298}^{1074} nC_p(NaCl)\,dT + n\Delta H_{1074}(NaCl) + \int_{1074}^{T_{ad}} nC'_p(NaCl)dT + \int_{298}^{1044} nC_p(KCl)\,dT + n\Delta H_{1044}(KCl) + \int_{1044}^{T_{ad}} nC'_p(KCl)dT \quad (4)$$

Fig. 2 showed the effect of NaCl and NaCl-KCl as diluents on the adiabatic temperature of ZrO_2-B_2O_3-Mg system. The adiabatic temperature of the system gradually decreased with the increase of the amount of diluent added. The T_{ad} reduced from 3090 K to 1949 K with 60 wt.% NaCl and 2028 K with 60 wt.% NaCl-KCl as the diluent. In comparison of the two diluents, NaCl had a better effect on reducing the adiabatic temperature for the same addition amount. When the amount of diluent was 70 wt.%, the reaction didn't occur in the actual experiment.

Phase composition of ZrB_2 powder

Fig. 3 was the XRD images of ZrB_2 prepared by adding different diluents. In Fig. 3a, the main phases before washing were ZrB_2, MgO and NaCl with addition of NaCl. And the main phases were ZrB_2, MgO, NaCl and KCl with addition of NaCl-KCl. No obvious reactant phase was observed in each group of samples, which indicated that the reaction was sufficient. When the addition amount of NaCl and NaCl-KCl was 0~60 wt.%, the combustion synthesis reaction of ZrO_2-B_2O_3-Mg system could be carried out normally, the reaction was sufficient and the excess Mg was also completely volatilized. Here, diluent salt phase appeared in each group, indicating that the diluent was not completely volatilized during the reaction.

In Fig. 3b, the final product after washing was pure ZrB_2 only when the NaCl addition was 60 wt.%, while slight $Mg_{0.2}Zr_{0.8}O_{1.8}$ phase appeared in other samples. According to the relative peak intensity of impurity phase and main phase, the content of impurity phase was low. After the initial product obtained by the salt-assisted combustion synthesis was washed, the by-product MgO

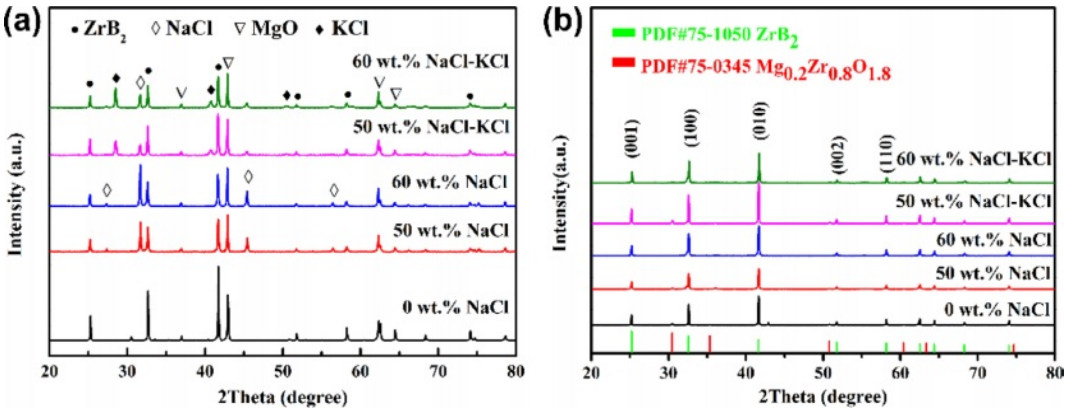

Fig. 3. XRD patterns of ZrB_2 with different diluents: (a) before washing, (b) after washing.

Table 3. The element content of ZrB_2 with different diluents.

Diluent	Zr (at.%)	B (at.%)	Mg (at.%)
0 wt.% NaCl	32.21	67.79	-
60 wt.% NaCl	30.97	68.27	0.76
60 wt.% NaCl-KCl	35.18	63.47	1.35

and residual salt were completely removed, but the impurity phase $Mg_{0.2}Zr_{0.}8O_{1.8}$ couldn't be removed by hydrochloric acid [41]. The reason for the formation of $Mg_{0.2}Zr_{0.8}O_{1.8}$ phase was the intermediate product of insufficient reduction of ZrO_2 by Mg. When the NaCl addition was 60 wt.%, a large amount of molten salt provided liquid mass transfer for the reaction, which was beneficial to the full reaction of Mg and ZrO_2.When the NaCl-KCl addition was 60 wt.%, a small amount of impurity phase appeared. This was because the viscosity of the mixed molten salt was higher than that of the single molten salt [44, 45], resulting in a slower mass transfer rate and a part of $Mg_{0.2}Zr_{0.8}O_{1.8}$ phase remained.

Electron probe X-ray microanalyser (EPMA) was selected to detect the element composition of ZrB_2 in each group. The test results in Table 3 indicated that the samples contained Zr, B and Mg elements. The ratio of Zr to B in other samples was close to 1:2, indicating that the phase was ZrB_2. From the XRD results, it is found that the samples with high Mg content exhibit high peak strength of $Mg_{0.2}Zr_{0.8}O_{1.8}$ phase in the XRD patterns, which indicated that Mg exists in the form of $Mg_{0.2}Zr_{0.8}O_{1.8}$. The content of Mg was the lowest with addition of 60 wt.% NaCl, and the purity of ZrB_2 was 99.24%, while the purity of ZrB_2 was 98.65% with addition of 60 wt.% NaCl-KCl mixed salt.

Table 4. Surface element atomic ratio of ZrB_2 with different diluents.

Diluent	Zr (at.%)	B (at.%)	O (at.%)	Mg (at.%)
60 wt.% NaCl	10.54	25.39	62.22	1.86
60 wt.% NaCl-KCl	10.05	24.81	62.63	2.05

XPS was used to analyze the surface elements of ZrB_2 prepared with different diluents. Fig. 4a showed the XPS full spectrum analysis. It could be seen that the surface elements of ZrB_2 include Zr, B, O and Mg. This indicated that Zr and B were the main elements of the product, O and Mg were impurity elements. The specific atomic ratio of each element was listed in Table 4. It could be found that the ratio of Zr and B was close to 1:2, and B was slightly excessive. It showed that the main chemical state of these two elements was ZrB_2, but there was still a small amount of B enriched on the surface under other chemical states. It was also found that the content of Mg was relatively small. According to the previous analysis, it was inferred that Mg existed in the product in the form of $Mg_{0.2}Zr_{0.8}O_{1.8}$ or $Mg_3B_2O_6$. According to the literature findings, the presence of $MgZrO_x$ and $Mg_3B_2O_6$ does not exert any detrimental impact on the utilization of ZrB_2 in high temperature ceramic applications [6, 46]. The content of O element was the highest. Except for the impurity phase formed by the reaction with other elements, a large part of it comes from the surface oxidation of ZrB_2 particles exposed to air.

Fig. 4b was the relative content of high resolution XPS spectra and chemical states of B1s and Zr3d peaks after ZrB_2 washing treatment. Fig. 4b showed that the 3d level of Zr shows typical $3d_{5/2}$ and $3d_{3/2}$ spin orbital splitting, while the B 1s showed typical single peak, which clearly indicated that there were two different bonding states between Zr and B atoms. In the product ZrB_2 powder, the binding energies of a group of $Zr3d_{5/2}$, $3d_{3/2}$ doublet states and B1s singlet state were 176 eV, 178.4 eV and 185.1 eV, respectively [47]. Another group of doublet and singlet states appeared at higher binding energies (180.2 eV, 182.6 eV and 189.9 eV), which were caused by ZrO_2 and B_2O_3 [47]. The content of B_2O_3 in B1s peak was higher when NaCl was added as diluent in Fig. 4c. According to the calculated adiabatic temperature and Gibbs energy, the adiabatic temperature of the system with addition of 60 wt.% NaCl was 1949 K, This was

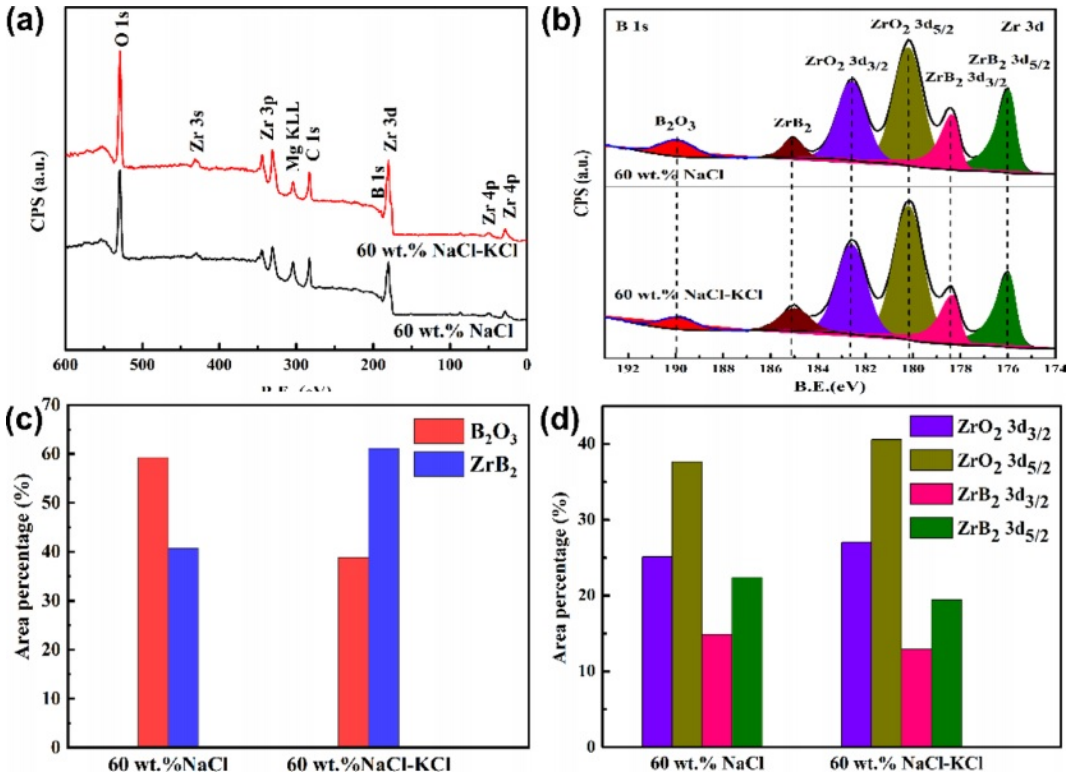

Fig. 4. (a) XPS full spectra, High resolution XPS spectra (b) and relative chemical content of B1s (c) and Zr3d (d) peaks of ZrB_2 with different diluents.

100 K lower than adding NaCl-KCl. At this temperature, the Gibbs energy of the magnesium thermal reduction reaction was greater than zero, and the inverse reaction trend increased. Moreover, it was not conducive to the binding of free B and Zr to generate ZrB_2 at a lower temperature. Therefore, when NaCl was used as diluent, the B_2O_3/ZrB_2 ratio of the product was larger. Fig. 4d showed that the ZrO_2/ZrB_2 of both samples were greater than 1.0, and the ZrO_2/ZrB_2 was larger when NaCl-KCl was added. This indicated that the content of ZrO_2 was higher, which was closely related to the oxidation of ZrB_2 particles.

Particle size and microstructure of ZrB_2 powder

Fig. 5 was the SEM image of ZrB_2 powder prepared by adding different diluents after immersion treatment. It could be seen from Fig. 5a that ZrB_2 particles prepared without diluents were coarse, and the particle size was generally above 1.0 μm. The particle shape were irregular and agglomeration was serious. In Fig. 5b, the ZrB_2 sample with addition of 60 wt.% had spherical and rectangular particles, and particle size was small, but there were adhesion and agglomeration between particles. It could be seen from Fig. 5c, the ZrB_2 particles with addition of 60 wt.% NaCl-KCl were finer and more uniform, most of the particle size were about 100 nm, the morphology was mainly spherical with good dispersion.

The particle size distribution was showed in Fig. 6. It could be found more intuitively that the particle size of ZrB_2 powder decreased with the increase of the amount of diluent. The product had the smallest particle size, more uniform distribution and more regular morphology with addition of 60 wt.% NaCl-KCl. According to the thermodynamic calculation, the adiabatic temperature of

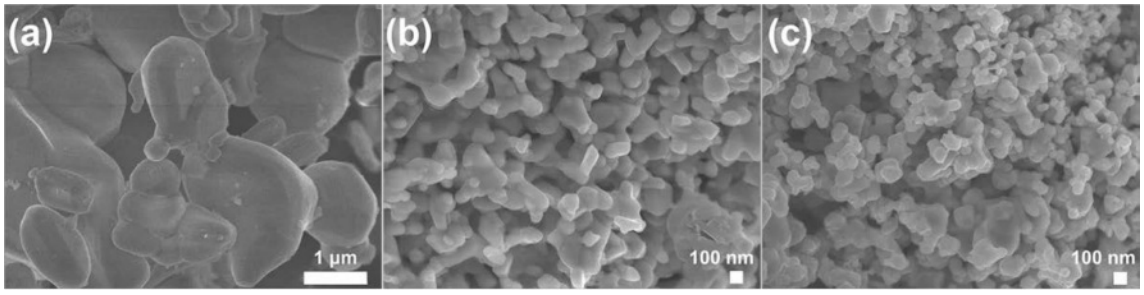

Fig. 5. SEM images of ZrB_2 with different diluents: (a) 0 wt.% NaCl, (b) 60 wt.% NaCl, (c) 60 wt.% NaCl-KCl.

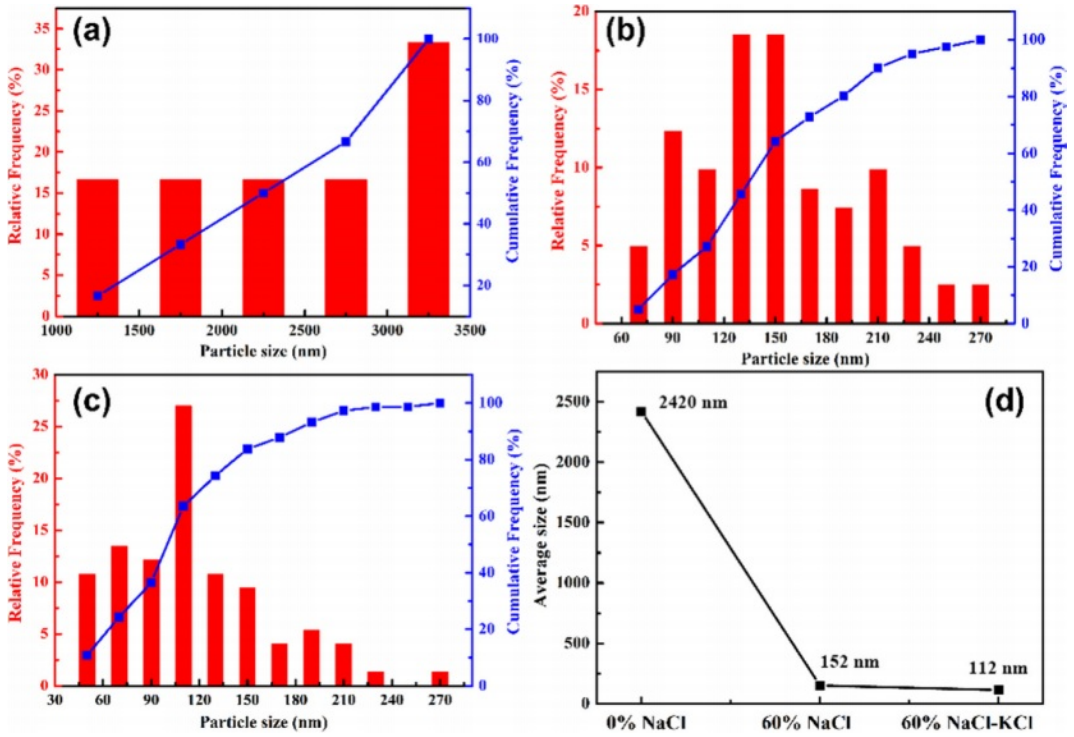

Fig. 6. The particle size distribution of ZrB_2 with different diluents: (a) 0 wt.% NaCl, (b) 60 wt.% NaCl, (c) 60 wt.% NaCl-KCl, (d) average particle size of ZrB_2 samples.

the system without diluent was 3090 K, but it decreased to 1949 K and 2028 K with addition of 60 wt.% NaCl and NaCl-KCl, respectively. This resulted in the reaction at a lower temperature and reduced the growth rate of ZrB_2 particles. At the same addition amount, NaCl-KCl had higher specific heat and viscosity than NaCl [48, 49], which was beneficial to slow down the heating rate of the system and reduce the crystal growth rate. Therefore, adding NaCl-KCl as diluent could effectively reduce particle size.

The specific particle size indexes of each group of samples were listed in Table 5. The particle size of ZrB_2 powder could be controlled from 2.0 μm to below 100 nm by adding diluents. When 60 wt.% NaCl-KCl was added, the D10, D50 and D90 of ZrB_2 particles were 50 nm, 100 nm, and 179 nm, respectively. The minimum average particle size is 105 nm. According to the literature findings, for ZrB_2 and its composite ceramic materials, a reduction in grain size leads to enhanced sintering densification of the powder, thereby improving the mechanical properties and high-temperature thermal properties of the material [50, 51].

Fig. 7 showed the TEM images of ZrB_2 with different diluents. In Fig. 7a, particle size of ZrB_2 without salt was large, about 2.0 μm, and the morphology was extremely irregular. When 60 wt.% NaCl-KCl was added, ZrB_2 particles with particle size less than 150 nm were obtained, and the minimum particle size was 52 nm (Fig. 7b). The TEM results were consistent with the SEM particle size statistics. The crystal plane spacing of (001) and (100) planes measured from the high-resolution image in Fig. 7c was 3.54 Å and 2.75 Å, respectively, corresponding to the standard ZrB_2 crystal [53]. In addition, combined with selected area electron diffraction (SAED) diagram of Fig. 7d, it was determined to be hexagonal ZrB_2 particle [54].

In addition, the ZrB_2 powder prepared in other literatures was also compared in Table 6, and it was found that the ZrB_2 prepared in this paper possessed the smallest average particle size (~105 nm). Importantly, compared with the method reported in other literatures (high-temperature synthesis requires more than 1200 °C),

Table 5. Particle size index of ZrB_2 with different diluents.

Diluent	D10/nm	D50/nm	D90/nm	Average size (*d*)/nm
0 wt.% NaCl	1200	2256	3098	2421
60 wt.% NaCl	79	135	211	140
60 wt.% NaCl-KCl	50	100	179	105

Note: D10, D50 and D90 correspond to the particle size of the sample whose cumulative particle distribution reaches 10%, 50%, and 90%, respectively [52].

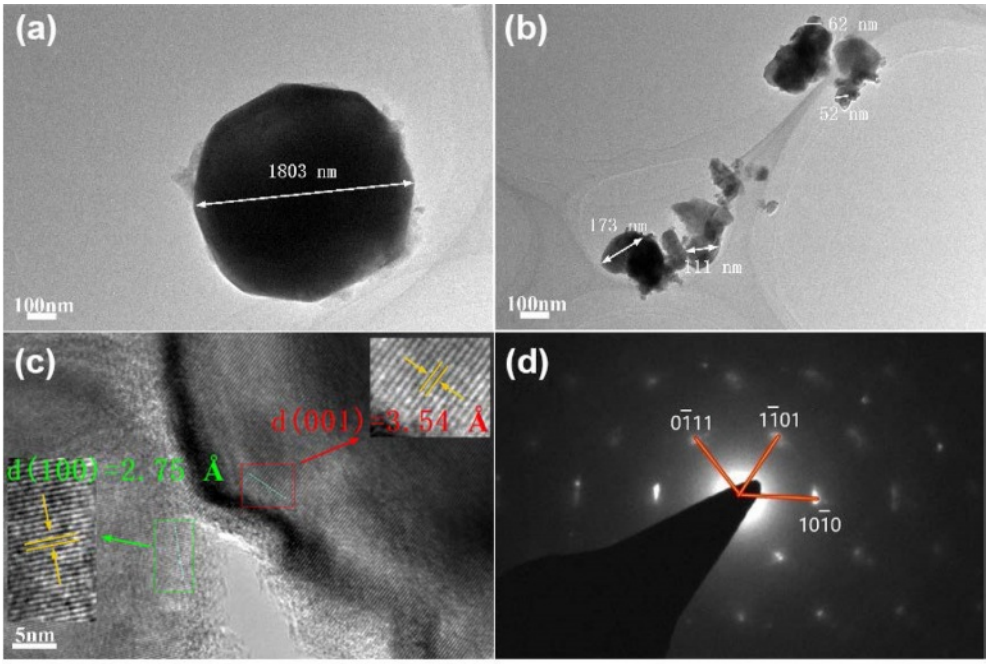

Fig. 7. The particle size distribution of ZrB_2 with different diluents: (a) 0 wt.% NaCl, (b) 60 wt.% NaCl-KCl, (c, d) HRTEM and SAED images of 60 wt.% NaCl-KCl.

Table 6. The comparison of ZrB_2 powder prepared in other literatures.

No.	Precursor	Process condition	Product quality	Ref.#
1	$Zr[OCH(CH_3)_2]_4$+H_3BO_3	1500 °C, 1 h	d = 100 nm	[16]
2	ZrO_2+B_4C+C	1800 °C, 4 h	d = 2-4 μm	[19]
3	ZrO_2+C+B_4C	1200 °C	d = 100 nm	[55]
4	ZrO_2+$Na_2B_4O_7$	1200 °C, 3 h	d < 0.7 mm	[56]
5	ZrO_2+B_2O_3+C	1550 °C, 0.5 h	d = 100-200 nm	[57]
6	ZrO_2+CaB_6	1200 °C	d = 200 nm	[58]
7	$ZrOCl_2{\cdot}8H_2O$+B_4C+C	1550 °C, 1 h	Rod-like ZrB_2 d > 30 μm	[59]
8	ZrO_2+B+B_4C	1650 °C, 1 h	d = 1.5-4.7 μm	[60]
9	$ZrSiO_4$+C+B_2O_3	1200 °C, 3 h	d = 500 nm	[61]
10	ZrO_2+B	1100 °C, 2 h	d = 200-500 nm	[62]

the self-spreading technology only needs to be ignited at ~250 °C to complete the preparation reaction, and the energy cost is lower. Some methods use organic raw materials, which are expensive and difficult to synthesize ZrB_2 powder on a large scale. In a comprehensive comparison, the technology in this paper has the advantages of low cost, low energy consumption and suitable for large-scale production, which provides convenience for nano-powders used in the device sintering of boride ceramics.

Formation mechanism of ZrB_2 nanopowder in diluent medium

The reaction process of ZrO_2-B_2O_3-Mg system was presented in Fig. 8. The initial mixture was placed in the reactor and preheated to the combustion temperature (533 K) of the ignition agent. The combustion of the ignition agent induced the materials to conducted magnesium thermal reduction reaction, and the self-propagating combustion heating stage began (Fig. 8a). As the temperature of the system increased, the melting point of B_2O_3 (723 K), Mg (923 K), and NaCl (1074 K) were reached successively. Liquid phase continuously appeared and the reaction degree was constantly intensified [63]. Liquid Mg reacted with ZrO_2 and liquid B_2O_3 respectively, and the heating rate of the system was accelerated (Fig. 8b). The micro reaction region became the heat source of the system and possessed the highest temperature. At the same time, NaCl phase transition absorbed heat and slowed down the heating rate of the system, making it the lowest temperature point in the system. In this case, the temperature field

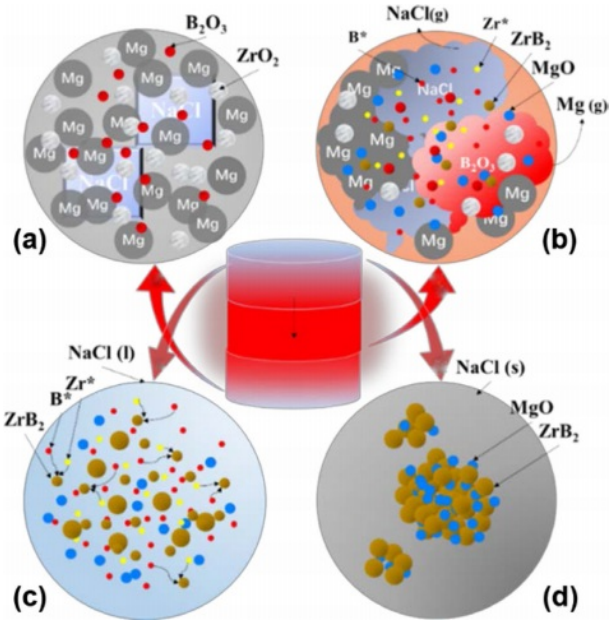

Fig. 8. Formation mechanism of ZrB_2 powder synthesized by salt-assisted combustion: (a) initial state, (b) temperature-rise period, (c) constant temperature stage and (d) cooling stage.

of the system exhibited a maximum temperature gradient [64]. When the heat release rate of the reaction and the heat absorption rate of NaCl reached equilibrium, the system reached the highest temperature [65]. After that, the system kept constant temperature at the NaCl crystallization point. During the constant-temperature process, NaCl continuously melted to provide sufficient liquid phase to coat the reactants and products, as shown in Fig. 8c. At this time, the free Zr* and B* migrated and diffused in molten salt, and combined to form ZrB_2 crystal nuclei after contact with each other. The small crystal nuclei continued to grow. However, due to the dilution and dispersion of NaCl, the molten salt surrounded the nucleated grains and inhibited the crystal growth [63]. The special molten salt environment was conducive to the nucleation and growth of ZrB_2 crystals into fine and uniform particles. Finally, at the cooling stage, the molten salt crystallized, the crystals stopped nucleating and growing [66], and all reactions completed, as shown in Fig. 8d.

Conclusion

In this paper, a new salt-assisted combustion synthesis process was proposed to prepare quasi-nanocrystalline ZrB_2 ultrafine powders by adding different diluents into ZrO_2-B_2O_3-Mg system. The two different diluents were single salt NaCl and mixed salt NaCl-KCl. The effects of the two diluents on the purity, particle size and microstructure of the product ZrB_2 were investigated as well as its mechanism. The quasi-nanocrystalline ZrB_2 powders with purity of 99.24% and 98.65% were obtained by adding 60 wt.% NaCl and NaCl-KCl, respectively. The impurity elements mainly existed in the form of $Mg_{0.2}Zr_{0.8}O_{1.8}$ phase and $Mg_3B_2O_6$ phase. Morphology and particle size analysis showed that both of two diluents could effectively reduce ZrB_2 powder particle size and obtain quasi-nanocrystalline powder with complete morphology and uniform particle size distribution. ZrB_2 power particle size could be controlled from 2.0 μm to below 100 nm by adding various diluents. Particle size of the product was the smallest with addition of 60 wt.% NaCl-KCl, and the D10, D50 and D90 of ZrB_2 particles were 50 nm, 100 nm, and 179 nm, respectively. The minimum average particle size is 105 nm. The salt-assisted combustion reaction degree, the mass transfer rate, crystal nucleation and growth rate were all affected by the phase transition temperature, specific heat and viscosity of diluents. This work will provide theoretical basis and technical support for large-scale preparation of boride nano-ceramic powders, which has broad application prospect.

Acknowledgements

This work was supported by the College Industry Support Plan of Gansu Province (2023CYZC-29), the Gansu Provincial Department of Education young doctor support project (2023QB-036), the China Postdoctoral Science Foundation (2022MD723787), the Open Fund of Gansu Key Laboratory of Solar Power System Engineering Project (2022SPKL04), and the Tamarisk Outstanding Young Talents Program of Lanzhou University of Technology (062202).

References

1. F.Q. Zhan, H. Zhang, K. Xv, M. Zhu, Y.H. Zheng, and P.Q. La, J. Ceram. Process. Res. 23[5] (2022) 694-708.
2. Y. Zhang and H. Sun, J. Ceram. Process. Res. 19[4] (2018) 355-359.
3. J.H. Kimb, J.S. Choia, J.U.K. Hura, S.C. Choia, and G.S. Ana, J. Ceram. Process. Res. 21[3] (2020) 351-357.
4. G.M. Yuan, X.H. Zuo, Z.J. Dong, Z.W. Cui, and X.K. Li, J. Ceram. Process. Res. 22[1] (2021) 31-38.
5. E.P. Aa, J. GRa, V. Sb, and A.B.J. Sc, J. Ceram. Process. Res. 21[5] (2020) 524-532.
6. M.H. Bagherabadi, R. Naghizadeh, H.R. Rezaie, and M.F. Vostakola, J. Ceram. Process. Res. 19[3] (2018) 218-223.
7. S. Gadakary, M.J. Davidson, R. Veerababu, and A.K. Khanra, J. Min. Metall. B. 52[1] (2016) 69-76.
8. M. Li and J. Zhang, J. Solid. State. Chem. 289 (2020) 121529-121532.
9. T. Gui, X.M. Wang, L. Yang, Y.Y Liu, X. Bai, L.J. Wang, and B. Song, Rare Metals. 37[12] (2018) 1076-1081.
10. H. Jin, S.H. Meng, C.H. Xu, J.H. Niu, and W.H. Xie, Ceram. Int. 42[14] (2016) 16354-16358.
11. X. Liu, C. Wei, L. Feng, J. Niu, and Z. Yang, Ceram. Int. 43[8] (2017) 6612-6617.
12. A.M. Stolin, P.M. Bazhin, A.S. Konstantinov, A.P. Chizhikov, and E.V. Kostitsyna, Ceram. Int. 44[12] (2018) 13815-13819.
13. R.Z. Wang, D.Y. Li, A. Xing, B. Jia, and W.G. Li,

Compos. Struct. 162 (2017) 39-46.
14. L. Bai, Y. Ouyang, and F. Yuan, Nanomaterials. 11[9] (2021) 2345-2362.
15. V. Zamora, A.L. Ortiz, F. Guiberteau, and M. Nygren, J. Eur. Ceram. Soc. 32[10] (2012) 2529-2536.
16. M. Rahmani-Azad, A. Najafi, N. Rahmani-Azad, and G. Khalaj, J. Sol-Gel. Sci. and Techn. 103[1] (2022) 87-96.
17. B.Y. Yang, J.P. Li, B. Zhao, Y.Z. Hu, and T.Y. Wang, Powder Technol. 256 (2014) 522-528.
18. J.H. Liu, S. Du, and F.L. Li, J. Wuhan. Univ. Technol., 33 (2018) 1062-1069.
19. B.L. Liu, C.Q. Li, and Y.N. Wang, Eur. Phys. J-Spec. Topics. (2022) 1-8.
20. J.S. Han, G.S. An, and S.C. Choi, Mater. Today. Commun. 33 (2022) 104646-104651.
21. C.Q. Liu, X.J. Chang, Y.T. Wu, X. Li, and Y.L. Xue, Ceram. Int. 46[6] (2020) 7099-7108.
22. S. Cordova and E. Shafirovich, J. Mater. Sci. 53[19] (2018) 13600-13616.
23. C.L. Yeh and Y.H. Wang, Ceram. Int. 47[5] (2021) 11202-11208.
24. J. Ma, S. Cao, T. Li, Q. Chen, and D. Zhang, Mater. Sci. Eng. B-Adv. 261 (2020) 114698-114701.
25. P.Q. La, Y.J. Ou, S.B. Han, X.F. Lu, and Y.P. Wei, J. Mater. Eng. Perform. 43[7] (2015) 14-20.
26. W.W. Wu, G.J. Zhang, and Y. Sakka, J. Asian. Ceram. Soc. 1[3] (2013) 304-307.
27. L. Yuan, C. Wang, M. Bi, S.D. Ma, and X.L. Weng, Adv. Appl. Ceram. 118[7] (2019) 395-402.
28. G.S. An, J.S. Han, J.U. Hur, and S.C. Choi, Ceram. Int. 43[8] (2017) 5896-5900.
29. H. Moayyeri, R.M. Aghdam, Ghelich, and F. Golestani-fard, Adv. Appl. Ceram. 117[3] (2018) 189-195.
30. M. Baris, T. Simsek, T. Simsek, S. Ozcan, and B. Kalkan, Adv. Powder. Technol. 29[10] (2018) 2440-2446.
31. Y. Wang, Y.D. Wu, K.H. Wu, S.Q. Jiao, K.C. Chou, and G.H. Zhang, Int. J. Min. Met. Mater. 26[7] (2019) 831-838.
32. M.B. Lee, J. Ceram. Process. Res. 19[2] (2018) 150-153.
33. A. Masoudian, M. Karbasi, F. SharifianJazi, and A. Saidi, J. Ceram. Process. Res. 14[4] (2013) 486-491.
34. X. Zheng, Q. Wang, X. Li, C. Zheng, and C. Shen, J. Ceram. Process. Res. 24[5] (2023) 874-883.
35. J.H. Lee, J.C. Park, B.S. Park, and H.K. Park, J. Ceram. Process. Res. 24[2] (2023) 216-221.
36. C. Kaemkit, S. Niyomwas, and T. Chanadee, J. Ceram. Process. Res. 21[4] (2020) 460-464.
37. V. Balouchi, F.S. Jazi, and A. Saidi, J. Ceram. Process. Res. 16[5] (2015) 605-608.
38. I. Barin, O. Knacke, and O. Kubaschewski, J. Chem. Thermodyn. 2013.
39. K.R. Kumar, K.K. Dama, and V.V. Satyanarayana, J. Ceram. Process. Res. 24[3] (2023) 439-445.
40. N. Ravikumar, R. Vijayan, and R. Viswanathan, J. Ceram. Process. Res. 24[1] (2023) 142-152.
41. B. Akgün, H.E. Çamurlu, Y. Topkaya, and N. Sevinç, Int. J. Refract. Met. H. 29[5] (2011) 601-607.
42. P.G. Ovcharenko, T.M. Makhneva, A.Y. Leshchev, V.V. Tarasov, and N.A. Balobanov, Met. Sci. Heat Treat 63[11] (2022) 629-633.
43. M. Sharifitabar, J. Vahdati khaki, and M. Haddad Sabzevar, Int. J. Refract. Met. H. 47 (2014) 93-101.
44. C. Koop-Santa, A. Sanchez-Martinez, E.R. López-Mena, J.L.A. Ponce-Ruiz, and E. Orozco-Guareño, Ceram. Int. 47[23] (2021) 33315-33321.
45. S. Zhang and Y. Yan, Case. Stud. Therm. Eng. 25 (2021) 100973-100984.
46. E.A. A.Ş. Demirkıran, Surf. Coat. Tech. 116-119 (1999) 292-295.
47. A.L. Ortiz, V. Zamora, and F. Rodríguez-Rojas, Ceram. Int. 38[4] (2012) 2857-2863.
48. H.X. Liu, W.H. Song, Q. Xu, W. Ma, and Y. Bai, Int. J. Electrochem. Sci. 15[7] (2020) 6238-6248.
49. Q. Yan, Q. Fan, C. Liu, and Z. Jing, Thermochim. Acta 690 (2020) 178689-178706.
50. M. Thompson, W.G. Fahrenholtz, and G. Hilmas, J. Am. Ceram. Soc. 94[2] (2010) 429-435.
51. J.-H. Yuan, Q.-Y. Liu, Y. You, L.-Y. Zeng, M.-W. Bai, L.R. Blackburn, W.-M. Guo, and H.-T. Lin, Ceram. Int. 47[11] (2021) 15843-15848.
52. J. Miller, P. Mulligan, and C.E. Johnson, Powder Technol 375 (2020) 28-32.
53. C. Zhibo, Z. Xiaotong, L. Mingliang, W. Hailong, and L. Qiang, Ceram. Int. 45[11] (2019) 13726-13731.
54. M. Velashjerdi, M. Soleymani, H. Sarpoolaky, and A. Mirhabibi, Ceram. Int. 46[18] (2020) 28639-28651.
55. Y. Wang, Y. Li, X.-H. Yang, and G.-H. Zhang, J. Nanopart. Res. 24[12] (2022) 1-13.
56. M. Li, C. Ke, and J. Zhang, J. Alloy. Compd. 834 (2020) 155062-155067.
57. H. Shen, X. Li, C. Hu, Z. Wang, X. Hu, Y. Li, and J. Yan, Surf. Interfaces 25 (2021) 101162-101167.
58. Z.-B. Li, Y. Wang, H. Zhang, B. Chen, G.-H. Zhang, and K.-C. Chou, Mat. Sci. Eng. A-Struct. 825 (2021) 141870.
59. Z. Chen, T.S. Suzuki, and H. Wang, Ceram. Int. 49[17] (2023) 28030-28035.
60. J.-H. Yuan, Q.-Y. Liu, Y. You, L.-Y. Zeng, M.-W. Bai, L.R. Blackburn, W.-M. Guo, and H.-T. Lin, Ceram. Int. 47[11] (2021) 15843-15848.
61. F. Li, C. Tan, J. Liu, J. Wang, and Q. Jia, Ceram. Int. 45[7] (2019) 9611-9617.
62. L. Zhou, Q. Fu, D. Hu, J. Zhang, and Y. Wei, Corros. Sci. 183 (2021) 109331-109340.
63. D. Ding, B. Bai, G. Xiao, J. Luo, and X. Chong, Ceram. Int. 47[13] (2021) 18708-18719.
64. X. Li, S. Wang, D. Nie, K. Liu, S. Yan, and P. Xing, Diam. Relat. Mater. 97 (2019) 107458-107463.
65. X. Yi, Q. Li, S. Suzuki, S. Zhang, T. Nomura, and T. Akiyama, Ceram. Int. 45[8] (2019) 10021-10027.
66. S. Song, J. Sun, J. Zhou, C. Guan, and Z. Hu, CrystEngComm. 23[3] (2021) 671-677.